scientific reports



Design of rectangular patch antennas through machine learning

Irene Merino-Fernandez^{1,2⊠}, Javier del Pino^{1,2} & Sunil Khemchandani^{1,2}

This paper presents a comprehensive methodology for rectangular-patch antenna design optimization by integrating electromagnetic (EM) simulations, machine learning (ML) techniques, and dielectric material analysis. A dataset was automatically generated through the design and EM simulation of 1000 antennas in PathWave Advanced Design System (ADS) for frequencies ranging from 0.5 GHz to 10.5 GHz in 0.1 GHz increments, considering various substrate materials. The analysis revealed that a given substrate only yielded valid antennas—defined as having return losses above 10 dB and gains greater than 0 dB—within specific frequency ranges, whereas outside these ranges, the antennas were ineffective. This highlights the critical role of dielectric material selection in antenna design. Based on the generated dataset, we evaluated multiple algorithms and selected two artificial neural networks (ANNs). The first ANN accurately predicts the geometrical parameters of a rectangular patch antenna given a target frequency. The second ANN effectively estimates the antenna's return loss and gain based on the computed geometrical parameters. Finally, the proposed methodology was integrated into an AI-driven antenna design toolbox, which demonstrated a coefficient of autodetermination (R^2) greater than 0.95 and a mean squared error (MSE) less than 0.03 in both geometrical parameter determination and performance prediction, achieving results comparable to those of full-wave electromagnetic simulations. Moreover, the computational overhead of the conventional workflow cannot be quantified precisely, as it often involves an indefinite sequence of electromagnetic (EM) simulations until the target performance is reached. In contrast, the machine-learning-assisted approach proposed here yields an antenna and its parameters within seconds, while requiring minimal computational resources.

The escalation of data rates and the expansion of coverage in modern mobile wireless communications systems pose significant challenges. Microstrip patch antennas stand out as prominent innovations in this domain because of their low cost, compact size, lightweight nature, ease of fabrication, and compatibility with printed circuit boards (PCBs)1. They find extensive applications in the wireless industry, including but not limited to airborne radar, radio telemetry, and satellite communications¹. The conventional approach to antenna design typically involves the following steps:

- The selection of a dielectric material, often flame retardant 4 (FR-4), is characterized by a dielectric constant (ϵ_r) and a thickness (h).
- The physical parameters, including the antenna's feeding point, are calculated via mathematical equations.
- Electromagnetic (EM) simulations are performed to obtain antenna parameters such as gain, bandwidth, radiation pattern, beamwidth, polarization, and impedance. It is common for the final antenna design to require optimization through iterative adjustments of physical parameters to obtain the desired response. The geometry optimization process is time-consuming as it is a multiobjective optimization with several variables to account for. In addition, the method relies on the designer's experience and requires extensive simulations following a trial-and-error methodology². Consequently, this manual approach consumes considerable computational resources and time³.

This paper proposes an artificial intelligence-based solution to improve design efficiency and alleviate the burden on human efforts. By leveraging artificial intelligence (AI), this approach aims to streamline the antenna design process, reducing reliance on manual optimization and accelerating the attainment of desired performance metrics. Some studies in the literature have shown the application of AI to antenna design.

First, a k-nearest neighbors' algorithm was applied in to predict the response of the antenna in terms of return loss (S_{11}) . Three antennas were considered: a circular patch antenna, a fractal antenna and a pyramidal horn antenna. Each antenna is characterized by different geometrical parameters, some of which are varied to

¹Instituto de Microelectrónica Aplicada, Universidad de Las Palmas de Gran Canaria (ULPGC), Parque Cientifico Tecnologico, 35017 Las Palmas de Gran Canaria, Spain. 2These authors contributed equally: Irene Merino-Fernandez, Javier del Pino and Sunil Khemchandani. email: imerino@iuma.ulpgc.es

obtain training data via an EM solver. Then, a machine learning (ML) model was trained and validated on the test data. Finally, the predicted output was compared with the EM solver response. However, the study does not specify the dielectric material used, making it difficult to assess the practical feasibility of the proposed designs.

Another approach is shown in³. This paper presents a method that begins by classifying the type of antenna to be designed via a support vector machine (SVM) model. The classification is based on performance requirements such as gain, bandwidth, resonant frequency, and S_{11} . A second model subsequently provides detailed geometric specifications to meet the identified requirements. To accomplish this, the significant variables were selected and varied in EM simulations to obtain the dataset. Then, the classification model is trained. Finally, the second model is trained by experimenting with various ML algorithms ultimately selecting the stacking ensemble learning approach. The same method was applied in⁵, but the k-nearest neighbors' algorithm was used to select between a square patch antenna, a pyramidal horn antenna and a helical antenna. Then, another algorithm obtains the geometrical parameters. In this study, dielectric parameters are swept arbitrarily during simulations without ensuring that the resulting configurations correspond to physically realizable substrate materials. Building on this approach, 6 introduces a four-layer feedforward ANN trained using the Levenberg-Marquardt algorithm to design microstrip patch antennas with square, triangular, and trapezoidal geometries. Unlike earlier models that focus solely on predicting physical dimensions, this network is capable of estimating both the patch dimensions and the optimal feed point, directly from performance parameters such as resonance frequency, gain, and return loss. The main problem with this work is the limited size of the datasets employed: none of them exceeds 200 samples. In addition, the study employs a single commercial substrate (Polytetrafluoroethylene (PTFE)) without assessing whether it is the most suitable choice for the antenna configurations explored. Finally, in 7 the authors propose a ML methodology to predict the equivalent resonant circuit (LRC) of a meandered slot patch antenna. The authors generate a dataset through CST simulations, extract resonance frequencies and return losses, and compute equivalent inductance and capacitance values. A random forest regression model is then trained to predict S_{11} , L, and C from the antenna's slot dimensions. However, it is limited to a single commercial substrate (RT/Duroid 5880), which restricts the generalization of the method across different dielectric materials.

In8, a technique employing regression-based ML approaches was introduced for designing a square patch antenna with a slot. The dataset is generated through EM simulations, wherein the design parameters such as frequency, slot size, dielectric material, patch thickness, and length are varied. Three models were developed, each adjusting the inputs to produce a distinct output. One model yields the resonance frequency, another provides the length, and the third determines the slot size. Additionally, various ML regression algorithms have been tested, such ANN, SVM, and decision tree-based regression methods, to evaluate their performance in predicting antenna parameters. Ultimately, a physical antenna designed via their method was presented, along with its S_{11} measurement, which was compared with the results obtained from EM simulations. In addition, in a comparative analysis of four machine learning models: ANN, random forest (RandForest), decision trees (DTs), and support vector regression (SVR) for predicting the physical dimensions of rectangular patch antennas is presented. Using a dataset of 3111 samples generated through HFSS simulations, their results showed that the random forest model outperformed the others in terms of mean squared error. This paper highlights the growing role of diverse ML strategies in reducing design time and enhancing geometric prediction accuracy. While the study in considers four distinct substrate materials with relative permittivities of 2.1, 2.2, 2.94, and 4, no systematic analysis is conducted to determine the most appropriate substrate for each design scenario. In contrast, 9 restricts the entire dataset to a single material (FR4), which may limit the performance of the antennas. Another contribution is found in , where ML algorithms were employed to predict the resonance frequency of a rectangular patch antenna. This study selects a dielectric material and frequency range, generating the antenna dataset through EM simulations. After that, various algorithms are tested to determine the optimal performance in predicting the resonance frequency. Additionally, a prototype is shown in this study. The main limitation of this work lies in the use of one substrate (FR4), with no consideration of its effectiveness in terms of electrical performance for the intended dual-band application.

This paper presents an AI-driven toolbox for designing rectangular patch antennas using machine learning. Its key innovation is the use of two independent models: one predicts antenna dimensions from the target frequency, and the other estimates performance $(S_{11}, gain)$ from those dimensions. This modular strategy, aligned with the conventional design workflow, outperforms a single deep model by improving generalization and simplifying training. Most state-of-the-art studies do not prioritize selecting the optimal dielectric material. For example, in⁴, the dielectric is not specified. In Refs.^{3,5} the parameters of the dielectric are swept, regardless of whether the material exists. In Refs. 1,6-9, a specific material was employed without ensuring its suitability as the optimal choice. The main idea of this paper is to work with commercial materials, compare the results obtained in terms of S_{11} and gain to choose the best option. This toolbox incorporates multiple commercial dielectric substrates and evaluates their suitability across different frequencies. Histograms are employed to analyze the real operability range of each material, enabling the system to recommend the most appropriate substrate for a given frequency. By combining predictive modeling with material screening, the toolbox facilitates a practical, fast, and accurate antenna design process.

This paper is structured as follows: "Antenna design" describes the antenna design theory, including the physical parameters and the feeding. Additionally, a study of dielectric theory is included. Section "Machine learning" outlines the most important considerations to the ML design. Section "Toolbox description" provides a comprehensive description of the entire methodology, from frequency selection to complete antenna design. Experiments to verify the methodology are presented in "Experiments", while "Conclusion" summarizes the conclusions drawn from the study.

Antenna design

This section describes the common analytical design process for rectangular patch antennas^{10,11}. The most important parameter is the working frequency (f), followed by the substrate parameters, namely the dielectric constant (ϵ_r) and thickness (h).

Equations (1)-(5) outline the dimensions of a rectangular patch antenna¹⁰. To better illustrate the patch antenna geometry, Fig. 1 provides a physical representation of the antenna.

The rectangular patch antenna width (W) can be computed as described in Eq. (1)

$$W = \frac{c}{2f} \sqrt{\frac{2}{\varepsilon_r + 1}} \tag{1}$$

where f is the working frequency and ϵ_r is the dielectric constant of the material. To calculate the effective dielectric constant (ε_{eff}), Eq. (2) can be used:

$$\epsilon_{eff} = (\epsilon_r + 1)/2 + (\epsilon_r - 1)/2 \sqrt{(1 + 12 \ h/W)}$$
 (2)

where W denotes the width and where h and ϵ_r are the thickness and the dielectric constant of the substrate respectively. Using Eq. 3, the length of the patch (L) is calculated:

$$L = L_{eff} - 2\Delta L \tag{3}$$

where L_{eff} represents the effective length, which is determined via Eq. (4), and ΔL denotes the length extension, which is computed via Eq. (5):

$$L_{eff} = \frac{c}{2f\sqrt{\varepsilon_{eff}}}\tag{4}$$

$$\Delta L = 0.412h \frac{(\varepsilon_{eff} + 0.3)(\frac{W}{h} + 0.264)}{(\varepsilon_{eff} - 0.258)(\frac{W}{h} + 0.8)}$$
 (5)

where ε_{eff} is the effective dielectric constant, f is the working frequency, W is the width of the patch and h is the thickness of the substrate.

A key consideration in antenna design is the feeding point, as it determines the reflection coefficient (S_{11}) of the antenna, and affects the matching bandwidth directly. As illustrated in Fig. 1, there are two methods for feeding patch antennas.

- A microstrip line was used (Fig. 1a). This method is optimal when the feeding circuit and the antenna are on the same layer.
- A point inside the patch antenna is used (Fig. 1b). This method is used if the circuit feeding the antenna and the patch antenna are in different layers¹².

In this case, the chosen method uses a microstrip line. The dimensions of the microstrip line that feeds the antenna can be determined using Eqs. (6)– $(12)^{11}$:

• x_0 is the space between the antenna and the feeding microstrip line. It can be calculated with the Eq. (6)

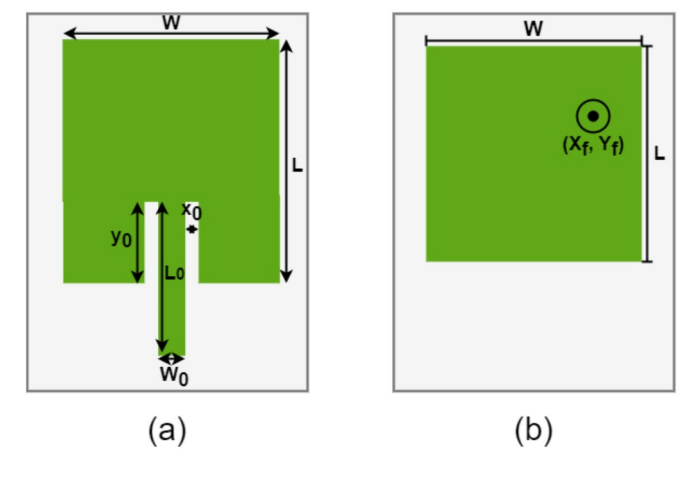


Figure 1. Patch antenna feeding methodologies: (a) microstrip line and (b) feeding Point.

$$x_0 = \lambda_0 / 100 \tag{6}$$

where λ_0 is the wavelength of the system.

• w_0 is the width of the microstrip. This is an important value because it determines the input impedance matching. It is calculated with Eq. (7)

$$Z_c = \frac{120\pi}{\sqrt{\epsilon_e f f} \left[\frac{W}{h} + 1.393 + 0.337 ln\left(\frac{W_0}{h} + 1.444\right)\right]}$$
(7)

where Z_c is the resonant input resistance without the impedance matching.

• y_0 is the insertion of the microstrip in the antenna. It can be calculated as shown in Eqs. (8)–(11).

$$R_{in}(y=y_0) = R_{in}(y=0)\cos^2\left(\frac{\pi}{L}y_0\right)$$
 (8)

$$R_{in}(y=0) = \frac{1}{2(G_1 \pm G_{12})} \tag{9}$$

$$G_1 = \frac{1}{120} \frac{W}{\lambda_0} \tag{10}$$

$$G_{12} = \frac{1}{120\pi^2} \int_0^{\pi} \left[\frac{\sin(\frac{k_0 W}{2}) \cos\theta}{\cos\theta} \right]^2 J_0(k_0 L \sin\theta) \sin^3\theta \, d\theta \tag{11}$$

where R_{in} is the input resistance, G_1 is the conductance of a single slot, G_{12} is the mutual conductance, k_0 is the wavenumber and J_0 is the Bessel function of the first kind of order zero. The \pm sign depends on the field distribution, where + represents odd distributions and - represents even distributions. In the case of the patch antenna, + is the selected sign.

• L_0 is the length of the feeding microstrip. Equation (12) was empirically defined in this study, since the length of the feeding line is phase-dependent and does not affect the antenna performance in this case.

$$L_0 = 2y_0 \tag{12}$$

The design expressions described above depend on the electrical properties of the dielectric materials used. Not all dielectric materials exhibit the same behavior across different frequency ranges, making the choice of dielectric crucial for achieving optimal antenna performance.

Dielectrics are materials with a low capacity to conduct electricity but support dielectric polarization when placed in an electric field. Positive charges align with the field direction, whereas negative charges align in the opposite directions. In antenna design, not all dielectric materials are suitable for all frequency designs because of several factors.

First, dielectric materials are characterized by their permittivity or dielectric constant, which is frequencydependent. At lower frequencies, the material charges have more time to align and polarize. This alignment does not occur at higher frequencies¹³. Consequently, the dielectric constant is inversely proportional to the frequency¹⁴. Additionally, the thickness of the dielectric affects the frequency in the same manner. As the thickness increases, the operational frequency decreases because of the fringing effect¹⁴. This effect arises from the air gap in the magnetic field and is influenced by frequency¹⁵, as the waves travel through both the dielectric and the air because of the finite antenna dimensions¹⁴.

Another factor to consider is the dielectric loss tangent, which indicates the dissipation of electrical energy caused by various physical processes, such as electrical conduction or dielectric resonance¹⁶. Materials with higher loss tangents dissipate more energy, making them less suitable for higher frequencies.

After reviewing the necessary antenna theory for this paper, we delve into machine learning and the techniques that will be employed in this study.

Machine learning

The term ML is one of the fundamental topics of AI. It uses existing information, following the strategy of supervised learning, to learn and generate a model, so that new data can be predicted¹⁷. The main goal involves the development of mathematical models capable of being trained with relevant data from an environment to determine the future without knowing all the external influence information¹⁷.

There are different algorithms available, such as linear regression, logistic regression, SVM and Naïve Bayes. In this case, three regression algorithms have been tested: ANN, RandForest, and SVR. This section provides an overview of the algorithms tried.

Artificial neural network

An ANN is a structured network that links an input layer to an output layer 17,18. It is composed of layers, which can be expressed as 18,19:

- Input layer. It obtains the features of the system to analyse. Typically these data are normalized to improve the numerical precision of the network.
- Hidden layers. They extracted the pattern of the analysed system by using *neurons*.
- Output layer. It is also formed by neurons, and provides the final network outputs, which are products of the previous layers.

ANNs can be implemented via different types of architectures, defining the organization of different neurons and their connections. Some of the architectures available are 18,19:

- · Single-layer feedforward architecture. This architecture has one input layer and a single output layer which also works as a hidden layer. These networks are used in pattern classification and linear filtering problems.
- Multiple-layer feedforward architecture. It is similar to the previous method but has multiple hidden layers. This is the solution for function approximation, pattern classification, system identification, process control, optimization, robotics, etc.
- Feedback architecture. This architecture has a particular output layer, as it feedbacks inputs for other neurons. These are employed in dynamic information processing.
- Mesh architecture. In this architecture, the spatial position of neurons is considered with the goal of pattern

Support vector regression

SVR is a ML technique derived from SVM, specifically adapted for regression problems. It is widely used in areas such as classification, regression, and signal processing. SVR is particularly effective in dealing with nonlinear and high-dimensional problems by applying the principle of local optimization^{20,21}.

The core idea behind SVR is to find a function f(x) that has at most ϵ deviation from the actual target values for all training data, while maintaining the model as flat as possible. The flatness is enforced by minimizing the norm of the weights, $||w||^2$, thus leading to better generalization capability^{21,22}.

Key components of SVR include:

- · Kernel function. SVR uses kernel tricks to transform input data into higher-dimensional spaces where linear separation is more feasible. Common kernels include linear, polynomial, and radial basis function (RBF).
- ϵ -insensitive loss. The model ignores errors smaller than ϵ , focusing only on predictions that lie outside the margin.
- Regularization parameter C. This controls the trade-off between the flatness of the function and the tolerance for deviations larger than ϵ . A smaller C allows more violations, while a larger C penalizes them heavily.

SVR is widely used in applications where accurate continuous prediction is required and the dataset may contain noise or nonlinear relationships²².

Random forest

RandForest is a powerful ensemble learning method used for both classification and regression tasks¹⁷. It often delivers performance comparable to advanced methods such as boosting and adaptive bagging. By incorporating random feature selection during training, RandForest enhances model robustness and accuracy, especially when working with large and complex datasets. Nevertheless, in certain scenarios, the method is susceptible to to overfitting, which may lead to noisy predictions or reduced generalization in both classification and regression tasks^{23,24}.

RandForest is composed of several key components^{24,25}:

- DT. Each tree is trained on a different subset of the original dataset, created through a process called bootstrap sampling. This means that some samples may be repeated, while others are left out.
- Random feature selection. At each split within a tree, a random subset of features is selected, rather than evaluating all of them. This increases diversity among trees and reduces overfitting.
- Aggregation mechanism. The final output is obtained by averaging the predictions of all trees (for regression) or taking the majority vote (for classification).

The main advantage of RandForest lies in its robustness and accuracy, especially when dealing with complex, high-dimensional datasets. It is less susceptible to overfitting than a single decision tree due to the averaging of multiple diverse models²⁵. However, in some cases, if the number of trees or the depth is too large, the model may still become overfitted or computationally expensive.

Toolbox description

This section provides a comprehensive description of the development of the proposed antenna design toolbox. Figure 2 graphically illustrates the workflow for better understanding. The process begins with the creation of the dataset, followed by the design of the ANNs and the analysis of histograms, concluding with the AI-driven antenna design toolbox.

Dataset generation

The dataset is created by combining MATLAB scripts with PathWave Advanced Design System (ADS) EM simulations. The automation of antenna layout generation is achieved via application extension language (AEL), the internal language of ADS. The patch antenna model used is shown in Fig. 1a. First, the physical parameters of the antennas (W, L, W0, L0, X0, Y0) are calculated following the procedure explained in "Antenna design". For

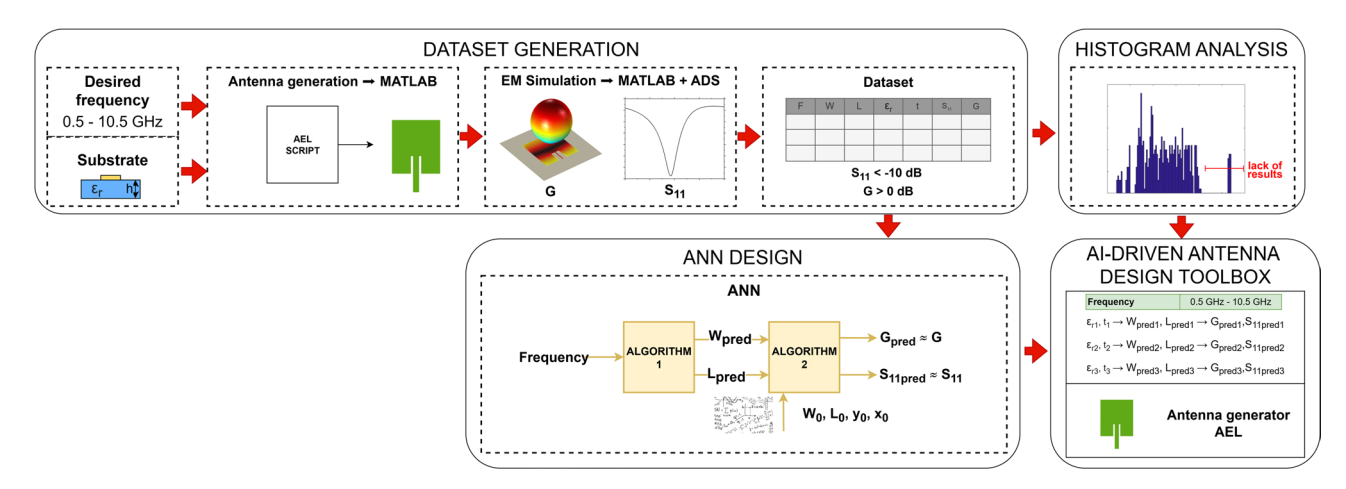


Figure 2. Methodology to create the AI-driven antenna design toolbox.

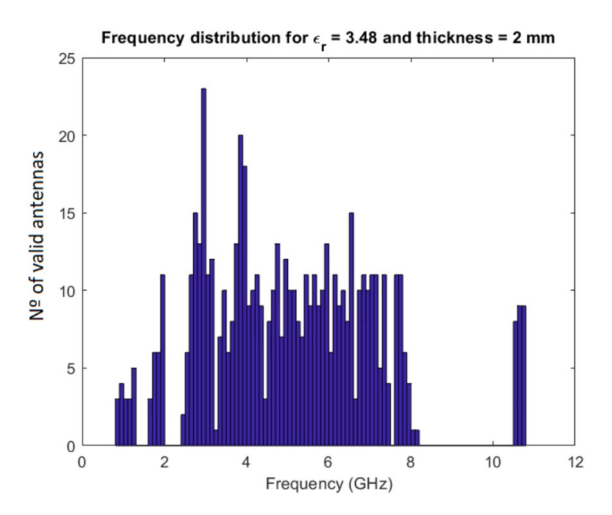


Figure 3. Histogram of valid antennas for a substrate with $\epsilon_r = 3.48$ and h = 2mm.

a given substrate, i.e. for a given ϵ_r and h pair, an antenna is generated for each frequency between 0.5 and 10.5 GHz in increments of 0.1 GHz, resulting in an initial dataset of 1000 antennas. Then, through AEL scripting, all the antenna layouts and EM simulation setups are created. Once all the EM simulations are executed, a dataset is compiled in a comma-separated values (CSV) file, and the frequency, gain, S₁₁, and physical parameters of each patch antenna are recorded. All EM simulations were performed using the ADS Momentum solver with default mesh settings, which offer a good trade-off between accuracy and computation time for this type of structure and frequency range.

Before the training process, the data need to be analysed, and nonoperational antennas, identified by S_{11} values exceeding -10 dB and gains below 0 dB, are removed from the dataset. For specific substrates, there are frequency ranges without valid antennas. This can be seen in the histogram which shows the number of functional antennas as a function of frequency. For example, Fig. 3 displays the histogram of functional antennas for a substrate with $\epsilon_r = 3.48$ and h = 2mm. It is evident that from 8 GHz to 10.5 GHz there are no data. This is because the dielectric material is not suitable for operation within that bandwidth or because the analytical equations lack precision in that range. Therefore, this information is saved in a database that records the frequency ranges in which each studied dielectric material does not produce valid antennas.

Once the data have been analysed, they are normalized by scaling the values in the range from 0 to 1. This ensures that the values are not excessively large, preventing neuron saturation during training. Finally, the dataset is divided into two subsets: training data and test data, at a ratio of 80:20.

ML design

This study addresses the problem by dividing it into two parts. The first aims to derive the geometrical parameters (W, L) from the desired frequency, while the second focuses on estimating the performance parameters (S_{11} and gain). The geometrical parameters of the microstrip line that feeds the antenna are determined analytically via the procedure explained in "Antenna design", based on the antenna's W and L, and the substrate properties ϵ_r and h. For this task, three machine learning (ML) algorithms were evaluated.

Artificial neural networks (ANN)

The ANNs applied in this work use a two-layer feedforward network architecture. Each network consists of an input layer, a hidden layer with a sigmoid transfer function, and an output layer with a linear transfer function. The optimal configuration was found to include 10 hidden neurons, selected manually by testing different values ranging from 5 to 15. This setup achieved the best trade-off between accuracy and generalization.

More complex deep neural networks (DNNs) were deliberately avoided. For instance, in⁹, the authors address a significantly more complex problem using a four-layer feedforward network with three hidden layers to manage a broader set of inputs. In contrast, such depth was not necessary in our case. Given the structured and low-dimensional nature of our input parameters, a simpler and more efficient approach was adopted.

This work implemented two independent feedforward neural networks: the first one predicts the antenna's physical dimensions (W, L), and the second estimates its performance metrics (gain, S_{11}) based on those dimensions. The proposed architectures are illustrated in Fig. 4.

Support vector regression (SVR)

In this study, an SVR model was implemented using MATLAB's fitrsvm function with a radial basis function (RBF) kernel. The input data was the normalized frequency, and the outputs $(W, L, gain, S_{11})$ were predicted independently using a one-output-per-model strategy. Hyperparameters such as KernelScale and BoxConstraint were optimized to minimize the validation error.

Random forest (RandForest)

In this work, the RandForest model was built using MATLAB's fitrensemble function with the Bag method. The algorithm was trained using normalized input frequency to predict the output vector composed of either antenna dimensions (W, L) or performance metrics (gain, S_{11}). Hyperparameter optimization via Bayesian search was applied to identify the optimal values for NumLearningCycles (number of learners), MaxNumSplits (maximum tree depth), and MinLeafSize (leaf size).

Results

For each commercial substrate material under evaluation, a set of independent neural networks or regression models was trained. The performance metrics reported - the mean squared error (MSE) and coefficient of determination (R^2) – correspond to the average values obtained from all trained models for each material.

This approach reduces the impact of model initialization variability and ensures that the reported results reflect a consistent and representative estimate of each model's predictive capacity across the entire dataset. Results are summarized in Table 1.

To evaluate the generalization capacity of the trained models, a 5-fold cross-validation procedure was applied. This method involves dividing the dataset into five equally sized subsets (folds). In each iteration, one fold is used as the test set while the remaining four folds serve as the training data. This process is repeated five times so that each fold is used once as test data. The final MSE obtained for the three algorithms is compared in Table 2.

For the design of patch antennas, the selected architecture is the ANN, which demonstrated the best overall performance among the evaluated models. This architecture is particularly well-suited for capturing complex nonlinear relationships between frequency and antenna characteristics. As shown in Tables 1 and 2, the ANN achieved the best values of MSE and R^2 in size prediction. Additionally, regularization techniques have been applied to improve generalization and prevent overfitting, thereby enhancing the model's performance on unseen data.

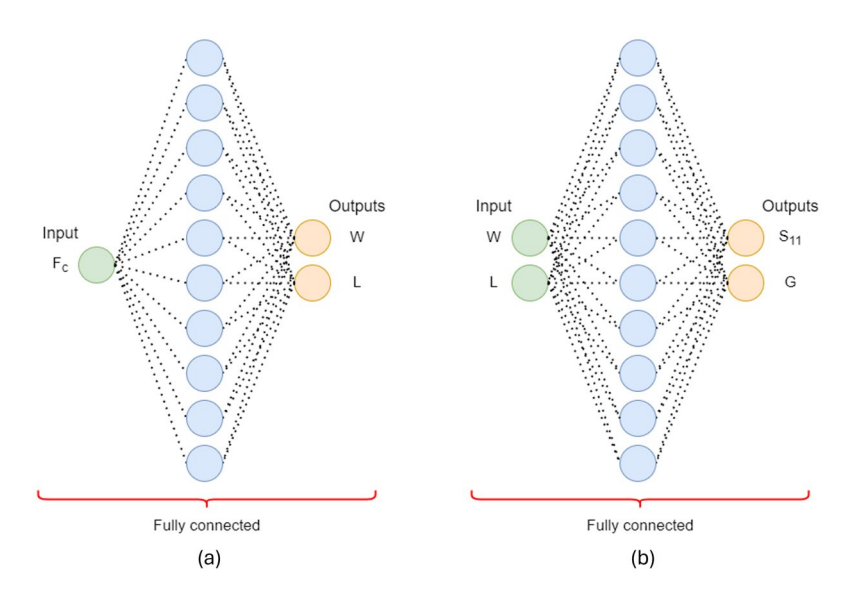


Figure 4. ANN architectures for deriving (a) geometrical parameters (W, L) and (b) performance parameters $(S_{11}, gain).$

Task	Metric	ANN	SVR	Random forest
Size	R^2	0.9803	0.9301	0.9306
Size	MSE	0.0009	0.0011	0.0011
Performance	R^2	0.9219	0.9137	0.9320
Teriormanee	MSE	0.0076	0.0029	0.0014

Table 1. Regression performance comparison of three machine learning models (ANN, SVR, and RandForest) for predicting antenna size parameters (W, L) and performance metrics (gain, S_{11}).

Model	Size	Performance			
ANN	0.0010	0.0260			
SVR	0.0012	0.0100			
RandomForest	0.0014	0.0208			

Table 2. Average MSE obtained through 5-fold cross-validation for each machine learning model: Artificial Neural Network (ANN), Support Vector Regression (SVR), and Random Forest (RandForest).

Material	ε_r	$ an \delta$	h (mm)
Shengyi Technology S1150G FR-4 ²⁶	4.6	0.011	0.05-3.2
Rogers RT/Duroid 6006 ²⁷	6.45	0.0027	0.635; 1.27; 1.9
Rogers RO3206 ²⁸	6.6	0.0027	0.64; 1.28

Table 3. Properties of materials used.

Although training time remained approximately constant across different configurations, hyperparameter tuning contributed to improved model stability. In particular, selecting appropriate values (e.g., the number of hidden neurons in the ANN or the tree depth in the RandForest) reduced fluctuations during training and improved generalization, as reflected in the validation metrics.

AI-driven antenna design toolbox

The proposed toolbox includes two key functionalities:

- · Material Listing: For each material, the geometrical and performance parameters are provided to help the user select the optimal antenna for a specific application. The commercially available materials implemented in this study include Shengyi Technology S1150G FR-4, Rogers RT Duroid 6006 and Rogers RO3206, each offered in various thicknesses. Table 3 summarizes the most important properties of these materials. These materials have been selected for their accessibility and proven reliability in antenna fabrication. They provide valid antenna designs either across the entire frequency range studied or within specific portions of it, depending on their dielectric properties and thicknesses.
- AEL Antenna Generation for ADS: Generates the layout, including the feeding point, ready to be simulated in ADS.

It is important to note that, in the proposed methodology, the substrate is not selected in advance by the user. Instead, the user simply provides a target operating frequency, and the toolbox internally evaluates all available substrates (with their respective ϵ_r and h values) and ranks them based on predicted performance. Substrate parameters were considered as additional input features during model development. However, it significantly degraded the predictive accuracy of the model, likely due to the increased dimensionality and nonlinear dependencies. Therefore, the final implementation keeps substrate selection implicit and data-driven. In practice, the toolbox evaluates all available trained substrates for the given frequency and provides the user with predicted performance parameters (W, L, S_{11} , and gain) for each material. The final choice is left to the user, who can take into account not only electrical performance but also practical aspects such as cost, availability, or fabrication preferences.

Experiments

To measure the quality of the models, two metrics are used: the \mathbb{R}^2 and the MSE.

The MSE measures the average squared difference between the predicted and actual values. As shown in Equation (13)²⁹, the MSE is calculated using the number of predictions (n) and the observed (E(θ)) and predicted (θ) values.

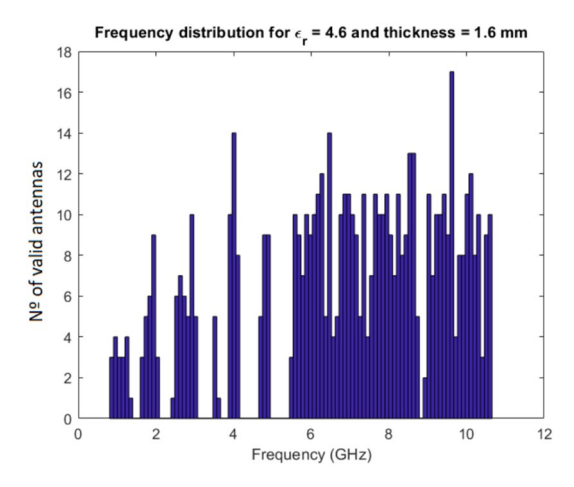


Figure 5. Histogram for valid antennas for a substrate with $\epsilon_r = 4.6$ and t = 1.6 mm.

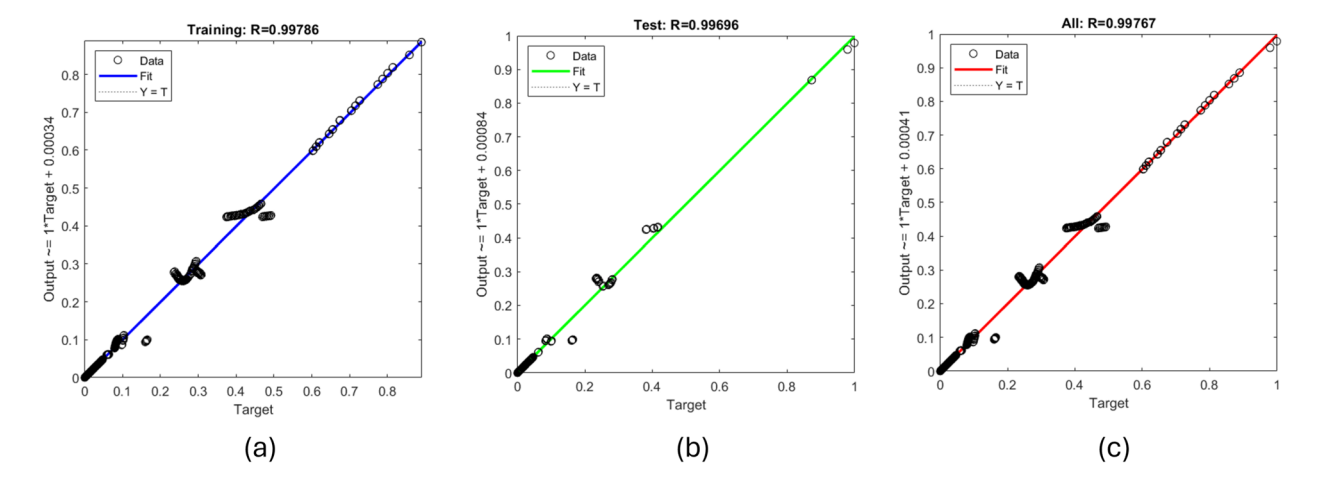


Figure 6. Regression plot for (a) training (b) test (c) all for $\epsilon_r = 4.6$ and t = 1.6 mm obtaining geometrical parameters W and L.

$$MSE = \frac{1}{n} \sum_{i=1}^{n} (E(\theta) - \theta)^{2}$$
 (13)

The R^2 measures how well a regression model fits the data. It is calculated as the ratio of the explained variance to the total variance 30 . As shown in Eq. (14), R^2 ranges from 0 to 1, with higher values indicating a better fit.

$$R^{2} = \frac{\sum_{i=1}^{n} (E(\theta) - \bar{\theta})^{2}}{\sum_{i=1}^{n} (\theta - \bar{\theta})^{2}}$$
(14)

As previously mentioned, for each dielectric material, an antenna was generated for each frequency between 0.5 GHz and 10.5 GHz in steps of 0.1 GHz, starting with an initial dataset of 1000 antennas. Figure 5 presents the histogram of functional antennas obtained for the first substrate analyzed, Shengyi Technology S1150G FR-4, with an ϵ_r of 4.6 and an h of 1.6 mm. As shown, this material exhibited 609 working antennas within a frequency range of 1 GHz to 10.5 GHz. However, the sample density begins to stabilize at approximately 5.5 GHz. The regression plots for the first ANN designed to predict geometric parameters are illustrated in Fig. 6. The MSEs for training and testing were 9.92×10^{-5} and 2.12×10^{-4} , respectively. Notably, the R^2 values were 0.998 for training and 0.997 for testing, indicating a perfect fit. Figure 7 depicts the regression plots for the second ANN designed to predict the performance parameters. The MSE for training was 0.0009, and for testing, it was 0.029. The \mathbb{R}^2 values were 0.9788 for training and 0.6604 for testing, suggesting a strong correlation between predicted and actual values.

To validate the generated models, three antennas were designed for frequencies of 3 GHz, 6 GHz, and 9 GHz for this substrate. Figure 8 compares the simulated and predicted S_{11} parameters for these antennas, revealing a larger error for the 3 GHz antenna. This is due to the substrate's limitations, which, as shown in Fig. 5, were

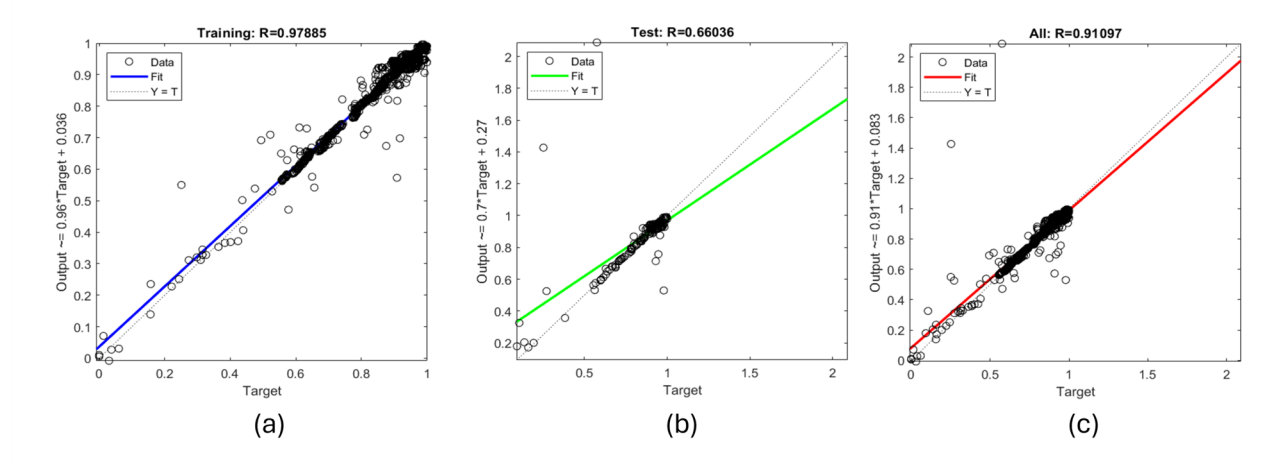


Figure 7. Regression plot for (a) training (b) test (c) all for $\epsilon_r = 4.6$ and t = 1.6 mm obtaining performance parameters S_{11} and gain.

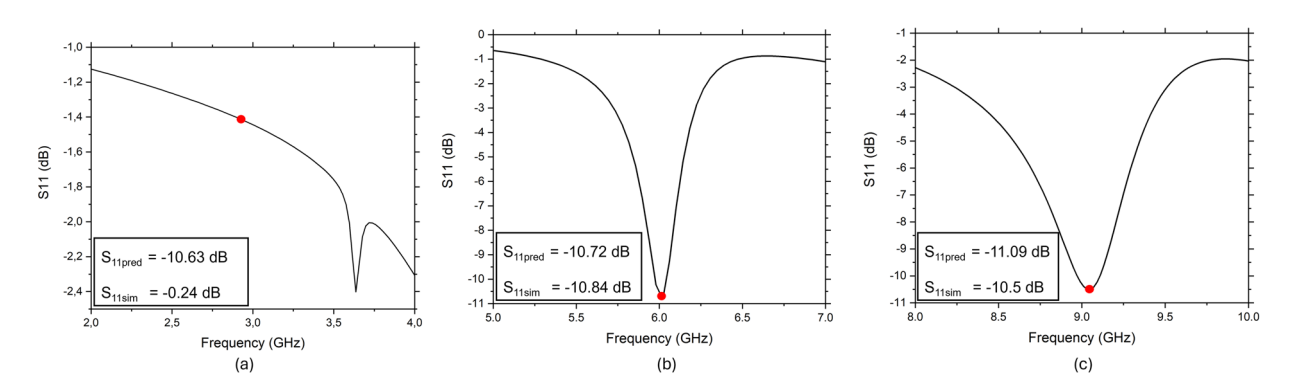


Figure 8. EM simulated S_{11} parameters for the (a) 3 GHz (b), 6 GHz (c) and 9 GHz antennas compared with those of the predicted model (red dots).

not suitable for frequencies below 3.5 GHz. Figure 9 shows the excellent agreement between the predicted and simulated gain values for the 6 GHz and 9 GHz antennas.

The same analysis was performed for different substrates. Table 4 summarizes the obtained results, where the 'pred' column corresponds to the predicted values and the 'sim' column corresponds to the simulated values. Additionally, the errors committed are summarized, with their absolute error (AE) and relative error (RE). Both error represents a consistent outcome. This validates the approach and suggests potential for other applications in related areas of study.

To verify the predictions and simulations, two antennas were manufactured using the same material as in the simulation: one designed for 6 GHz and the other for 9 GHz, as shown in Fig. 10. The 6 GHz antenna has physical dimensions of 15.2 mm × 14.9 mm, while the 9 GHz antenna measures 9.7 mm × 10.0 mm. These dimensions were directly obtained from the neural network model, ensuring that the fabricated prototypes match the layouts predicted during the design stage.

A Keysight Technologies N5225B PNA Microwave Network Analyser model was used to obtain the S-parameter results. The results obtained are presented in Fig. 11. The simulation and measurement results for the 6 GHz antenna (Fig. 11a) are highly consistent, with the S_{11} peak value being identical at -10.8 dB. For the 9 GHz antenna (Fig. 11b), the peak frequency of S_{11} was shifted by 250 MHz, with a peak value of -11.08 dB. At 9 GHz, the measured S_{11} value is -9.6 dB, while the peak value in the simulation is -10.5 dB.

Table 5 provides a comprehensive comparison of ML-based antenna design methodologies reported in the literature. The table summarizes the antenna types, ML techniques used, design objectives, substrate considerations, and whether the results were experimentally validated.

The analyzed studies cover a variety of antenna geometries, such as rectangular patches, circular horns, fractal and slot structures. In terms of ML techniques, there is a diverse range including traditional models like decision trees (DT) and regression, RandForest, SVR, and ANN, including convolutional neural networks (CNNs). Notably, hybrid or combined approaches are also explored, such as ensemble learning or models integrating both classification and regression.

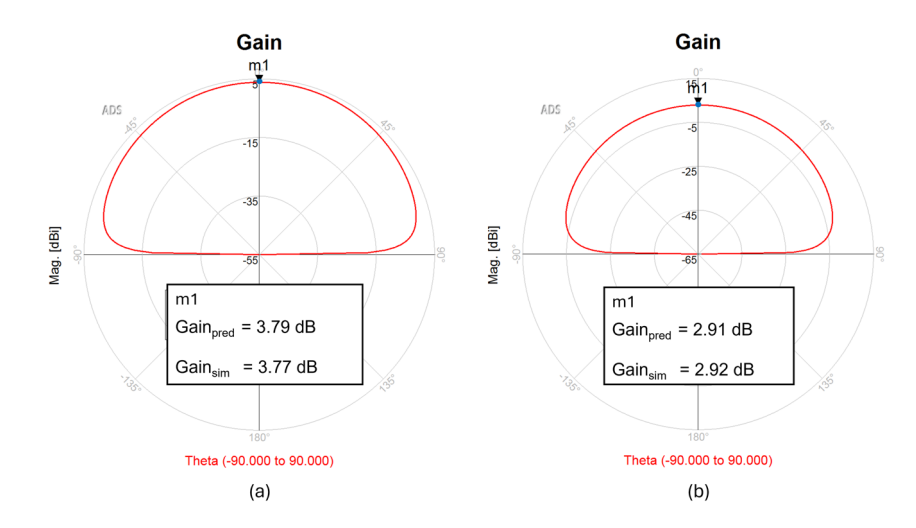


Figure 9. 2D cut far field simulated gain for the (a) 6 GHz and (b) 9 GHz antennas compared with those of the predicted model (blue dots).

	6 GHz - S ₁₁ (dB)				6 GHz - Gain (dB)			9 GHz - S ₁₁ (dB)				9 GHz - Gain (dB)				
Material	Pred	Sim	AE	RE	Pred	Sim	AE	RE	Pred	Sim	AE	RE	Pred	Sim	AE	RE
$\varepsilon_r = 4.6, t = 1.6 \mathrm{mm}$	- 10.72	- 10.82	0.1	0.009	3.77	3.79	0.002	0.005	- 11.09	- 10.5	0.41	0.03	2.91	2.92	0.01	0.003
$\varepsilon_r = 4.6, t = 2 \mathrm{mm}$	- 11.03	- 11.34	0.31	0.02	3.44	3.46	0.002	0.005	- 11.62	- 12.13	0.51	0.04	1.9	1.88	0.02	0.01
$\varepsilon_r = 4.6, t = 2.4 \mathrm{mm}$	- 11.73	- 11.83	0.1	0.008	2.93	2.93	0.000	0.000	- 11.10	- 11.59	0.49	0.04	0.87	0.86	0.01	0.01
$\varepsilon_r = 6.45, t = 1.27 \mathrm{mm}$	- 11.86	- 11.91	0.05	0.004	2.69	2.88	0.19	0.06	- 13.64	- 13.51	0.13	0.01	3.32	3.15	0.07	0.02
$\varepsilon_r = 6.45, t = 1.9 \text{ mm}$	- 13.92	- 14.49	0.57	0.03	2.71	2.65	0.06	0.02	- 13.28	- 13.06	0.22	0.02	0.74	0.60	0.09	0.14
$\varepsilon_r = 6.6, t = 1.28 \mathrm{mm}$	- 12.17	- 12.17	0.00	0.000	3.13	3.16	0.03	0.01	- 13.57	- 13.70	0.13	0.01	2.6	2.77	0.17	0.06

Table 4. Predicted (Pred) and simulated (Sim) S_{11} and gain for different substrates at 6 GHz and 9 GHz with their absolute errors (AEs) and relative errors (REs).

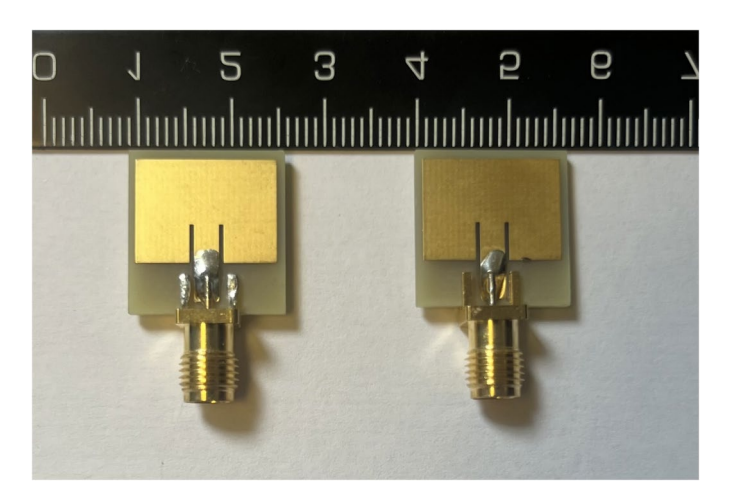


Figure 10. From left to right: 6 GHz antenna and 9 GHz antenna.

The design objectives vary widely-from predicting resonant frequency or S_{11} parameters to selecting antenna geometry or directly determining physical dimensions like W and L. This diversity reflects the flexibility of ML techniques in addressing different stages of the antenna design pipeline.

Regarding substrates, only a few works specify whether commercial or theoretical materials were used. Several studies sweep the dielectric constant ϵ_r without focusing on physically realizable materials, which may

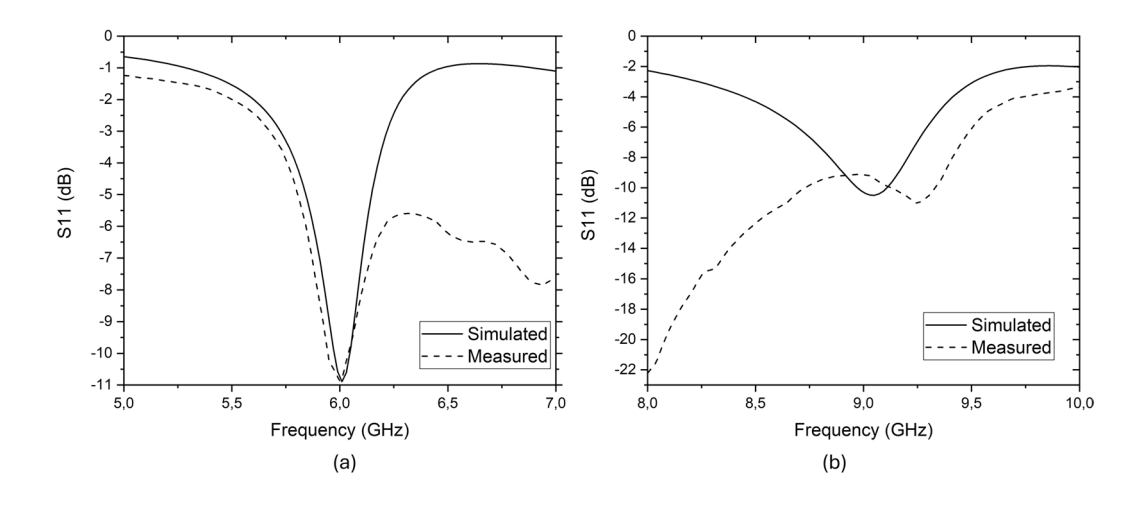


Figure 11. S_{11} simulated and measured results for the (a) 6 GHz and (b) 9 GHz antennas.

	1	3	4	5	8	6	7	9	This work
Antenna type	Rectangular Patch	Circular patch Horn Spiral	Circular Fractal Horn	Square Horn Helical	Slot Patch	Square Triangle Trapezoid	Meandered Slot	Rectangular Patch	Rectangular Patch
ML technique	CNN Linear regression RandForest DT Lasso regression Ridge regression XGB Regression	SVM + Stacking ensemble learning	K-NN	DT + Regression	RandForest SVR ANN DT	4-layer ANN	ML (unspecified)	ANN RandForest DT SVR	ANN RandForest DT SVR
Objective	Resonance frequency	Select antenna + geometry	Predict S_{11}	Select antenna + geometry	Geometry + frequency prediction	Geometry + feed point	Predict S_{11} + impedance	Predict W and L	Predict W and L + S ₁₁ and gain
Substrate	Not specified	Swept ε_r	Not specified	Swept ε_r	Commercial, multiple	Commercial, one	Commercial, one	Commercial, one	Commercial, multiple
Measured validation	Yes	No	No	No	Yes	Yes	No	No	Yes

Table 5. Comparison of ML-based antenna design methodologies.

compromise real-world applicability. This highlights the need for greater attention to material feasibility in MLdriven antenna design.

In terms of measured validation, some studies support their findings through physical prototyping and empirical measurements, whereas others depend exclusively on simulation results, which-despite their usefulness-may fall short in confirming real-world performance.

Compared to the existing literature, the present work offers several key advancements. First, unlike other studies that either focus on predicting a single electromagnetic parameter (such as S_{11} or resonant frequency) or treat geometry generation and performance prediction as isolated tasks, this work simultaneously predicts both physical dimensions (W and L) of the antenna and its performance (S_{11} and gain) from the desired frequency.

Moreover, while many prior works either do not specify the substrate or sweep the dielectric constant ε_r across non-commercial values, this work operates strictly with commercially available dielectric materials. This ensures that all predicted designs are practically feasible.

Unlike several references that rely exclusively on simulated data, this study includes a physical prototype fabricated using the predicted parameters. The experimental results are compared with simulation outcomes, providing strong evidence of the model's accuracy.

Finally, the methodology adopted in this work simplifies the modeling process. By focusing on a limited but well-chosen set of input parameters, the need for deep or overly complex neural network architectures is eliminated. Instead, simple but effective models are enough to make accurate predictions. This contrasts with other studies that rely on deeper networks or complex models to handle more extensive or unstructured inputs.

Conclusion

The integration of ML into rectangular patch antenna design offers a promising approach to streamline the design process and enhance efficiency. This study introduces a new methodology that not only automates iterative design steps but also generates an AEL file, allowing easy layout generation within ADS software. By automating the

iterative design process, ML algorithms significantly reduce human intervention and computational resources compared with traditional trial-and-error methods.

Furthermore, the proposed approach takes into account commercially available substrates, ensuring more practical and applicable results. This study underscores the critical importance of selecting appropriate dielectric materials for optimal antenna performance. It is evident that not all materials are suitable for all frequency ranges, leading to substantial inaccuracies in antenna behavior within certain frequency bands.

The proposed ML-based methodology demonstrates remarkable accuracy in calculating antenna geometrical parameters (W and L) and predicting performance metrics (return loss " S_{11} " and gain). The results obtained are comparable to those achieved through electromagnetic simulations.

This approach outlines significant opportunities for future advancements in the field of electromagnetic device optimization. This methodology could be extended to more complex antenna geometries, such as fractal, horn, or array configurations, which would further expand its applicability across a broader range of wireless communication systems. In addition to antenna design, this machine learning-driven approach may also be applied for the optimization of other radiofrequency (RF) and microwave components, such as filters, amplifiers, and phased arrays, where high precision and reduced design time are critical.

Regarding computational efficiency, the proposed ML-based approach offers significant advantages. For example, on a PC with an Intel Core i7-12700K @ 3.60 GHz and 32 GB RAM, the complete prediction process takes around 5 seconds. In contrast, the traditional workflow often requires hours of manual work, especially for non-experts, due to iterative EM simulations, substrate selection, feeding optimization, and validation. Even for skilled designers, reaching a well-matched antenna design can take more than 45 minutes. The ML toolbox not only accelerates the design process, but also removes the dependency on specialized knowledge.

Data availability

Datasets generated during the current study are available from the corresponding author on reasonable request.

Code availability

The custom code used to train and evaluate the models is not publicly available due to intellectual-property considerations. The code can be made available by the corresponding author upon reasonable request for academic, non-commercial purposes.

Received: 7 May 2025; Accepted: 4 September 2025

Published online: 29 September 2025

References

- Haque, M. A. et al. Dual band antenna design and prediction of resonance frequency using machine learning approaches. Appl. Sci. 12, 10505. https://doi.org/10.3390/app122010505 (2022).
- 2. Kurniawati, N., Fahmi, A. & Alam, S. Predicting rectangular patch microstrip antenna dimension using machine learning. J. Commun. 16, 394-399. https://doi.org/10.12720/jcm.16.9.394-399 (2021).
- 3. Shi, D., Lian, C., Cui, K., Chen, Y. & Liu, X. An intelligent antenna synthesis method based on machine learning. IEEE Trans. Antennas Propag. 70, 4965–4976. https://doi.org/10.1109/TAP.2022.3182693 (2022).
 4. Indharapu, S. S., Caruso, A. N. & Durbhakula, K. C. Supervised machine learning model for accurate output prediction of various
- antenna designs. In 2022 IEEE International Symposium on Antennas and Propagation and USNC-URSI Radio Science Meeting (AP-S/URSI), 495-496, https://doi.org/10.1109/AP-S/USNC-URSI47032.2022.9886262 (2022).
- 5. Ramasamy, R. & Bennet, M. A. An efficient antenna parameters estimation using machine learning algorithms. Prog. Electromagn. Res. C 130, 169-181. https://doi.org/10.2528/PIERC23011203 (2023).
- 6. Dhar, J. P., Hasan, M., Nīshiyama, E. & Toyoda, I. Microstrip patch antenna design using a four-layer feed forward artificial neural network trained by levenberg-marquardt algorithm. IEEE Access 13, 55244-55259. https://doi.org/10.1109/ACCESS.2025.3553913
- 7. Wang, Y. et al. Machine learning-based reflection coefficient and impedance prediction for a meandered slot patch antenna. Mater. Sci. Semicond. Process. 188, 109245. https://doi.org/10.1016/j.mssp.2024.109245 (2025).
- 8. Sharma, K. & Pandey, G. P. Efficient modelling of compact microstrip antenna using machine learning. AEÜ Int. J. Electron. Commun. 135, 153739. https://doi.org/10.1016/j.aeue.2021.153739 (2021).
- 9. Degachi, M. & Ghendir, S. Comparative analysis of machine learning models to predict rectangular patch antenna dimensions. J. Appl. Res. Technol. 22, 1131-1139. https://doi.org/10.1016/j.jart.2024.11.004 (2024).
- 10. Merino-Fernandez, I., Khemchandani, S., Pino, J. & Saiz-Perez, J. Phased array antenna analysis workflow applied to gateways for leo satellite communications. Sensors 22, 9406. https://doi.org/10.3390/s22239406 (2022).
- 11. Balanis, C. A. Antenna Theory: Analysis and Design (John Wiley & Sons, 2016).
- 12. Jasim, S. E., Jusoh, M. A., Mazwir, M. H. & Mahmud, S. N. S. Finding the best feeding point location of patch antenna using hfss. ARPN J. Eng. Appl. Sci. 10, 17444-17449 (2015).
- 13. Psarras, G. C. Fundamentals of dielectric theories. In Dang, Z.-M. (ed.) Dielectric Polymer Materials for High-Density Energy Storage, 11-57, https://doi.org/10.1016/B978-0-12-813215-9.00002-6 (William Andrew Publishing, 2018).
- 14. Choudhury, S. Effect of dielectric permittivity and height on a microstrip-fed rectangular patch antenna. Int. J. Electron. Commun. Technol. 5, 129-130 (2014).
- 15. El-Saadany, E. F. Magnetic circuits (2006). Technical report.
- 16. Sebastian, M. T. Measurement of microwave dielectric properties and factors affecting them. In Dielectric Materials for Wireless Communication, 11-47, https://doi.org/10.1016/B978-0-08-045330-9.00002-9 (Elsevier, 2008).
- 17. Bonaccorso, G. Machine learning algorithms: Popular algorithms for data science and machine learning (Packt Publishing Ltd,
- 18. Bishop, C. M. Pattern Recognition and Machine Learning (Springer, New York, 2006).
- 19. Silva, I. N., Spatti, D. H., Flauzino, R. A., Liboni, L. & Alves, S. Artificial neural networks: A practical course (Springer, 2016).
- 20. Rivera, G., Cruz-Reyes, L., Dorronsoro, B. & Rosete, A. Data Analytics and Computational Intelligence: Novel Models, Algorithms and Applications. Studies in Big Data (Springer Nature Switzerland, 2023).
- 21. Drucker, H., Burges, C. J. C., Kaufman, L., Smola, A. J. & Vapnik, V. Support vector regression machines. Adv. Neural. Inf. Process. Syst. 9, 155-161 (1997).

- 22. Smola, A. J. & Schölkopf, B. A tutorial on support vector regression. Stat. Comput. 14, 199-222. https://doi.org/10.1023/B:STCO.0 000035301.49549.88 (2004)
- Chandra, S. S. V. & Hareendran, A. S. Machine Learning: A Practitioner's Approach. Eastern Economy Edition (PHI Learning Private Limited, 2021).
- 24. Breiman, L. Random forests. *Mach. Learn.* 45, 5–32. https://doi.org/10.1023/A:1010933404324 (2001).
- 25. Breiman, L. Random forests. Mach. Learn. 45, 5-32. https://doi.org/10.1023/A:1010933404324 (2001).
- 26. Shengyi Technology Co., L. S1150g datasheet. Available online: https://www.shengyi-usa.com/halogen-free-lead-free-compatibl e-fr-4/. Accessed on 17 (February 2025).
- 27. Corporation, R. Rt/duroid* 6006 datasheet. https://www.rogerscorp.com/-/media/project/rogerscorp/documents/advanced-electr onics-solutions/english/data-sheets/rt-duroid-6006-6010lm-laminate-data-sheet.pdf. Accessed on 17 (February 2025).
- 28. Corporation, R. Ro3200™ series datasheet. https://www.rogerscorp.com/-/media/project/rogerscorp/documents/advanced-electro nics-solutions/english/data-sheets/ro3200-series-data-sheet.pdf. Accessed on 17 (February 2025).
- 29. MacKenzie, D. I. et al. Fundamental Principles of Statistical Inference, 71-111 (Academic Press, Boston, 2018), 2nd edn.
- 30. Freedman, D. A. Coefficient of Determination, 88-91 (Springer) (New York, NY, New York, 2008).

Acknowledgements

The authors would like to thank the editors and anonymous reviewers for providing insightful suggestions and comments to improve the quality of the research paper. The authors would like to express their gratitude to Ayoze Díaz Carballo for assisting in the development of the code used in this study. Special thanks to José Saiz Pérez for his guidance in defining the dielectric materials. We are also deeply thankful to Adrián Canella Ortiz for his support in defining and implementing the artificial neural networks. This work has been partially supported by the Spanish Ministry of Science and Innovation (MCIN) and the Research State Agency (AEI) as part of the project with ID PID2021-127712OB-C21/MCIN/AEI/10.13039/501100011033/FEDER, EU, and PDC2023-145828-C22/MCIN/AEI/10.13039/501100011033/NextGenerationEU, and by Universidad de Las Palmas de Gran Canaria by the PIFULPGC2020-2 ING-ARQ3 grant.

Author contributions

All the authors contributed equally to the conceptualization, design, data collection, analysis, and writing of this paper. All authors have read and approved the final manuscript.

Declarations

Competing interests

The authors declare no competing interests.

Additional information

Correspondence and requests for materials should be addressed to I.M.-F.

Reprints and permissions information is available at www.nature.com/reprints.

Publisher's note Springer Nature remains neutral with regard to jurisdictional claims in published maps and institutional affiliations.

Open Access This article is licensed under a Creative Commons Attribution-NonCommercial-NoDerivatives 4.0 International License, which permits any non-commercial use, sharing, distribution and reproduction in any medium or format, as long as you give appropriate credit to the original author(s) and the source, provide a link to the Creative Commons licence, and indicate if you modified the licensed material. You do not have permission under this licence to share adapted material derived from this article or parts of it. The images or other third party material in this article are included in the article's Creative Commons licence, unless indicated otherwise in a credit line to the material. If material is not included in the article's Creative Commons licence and your intended use is not permitted by statutory regulation or exceeds the permitted use, you will need to obtain permission directly from the copyright holder. To view a copy of this licence, visit http://creativecommo ns.org/licenses/by-nc-nd/4.0/.

© The Author(s) 2025

Terms and Conditions

Springer Nature journal content, brought to you courtesy of Springer Nature Customer Service Center GmbH ("Springer Nature").

Springer Nature supports a reasonable amount of sharing of research papers by authors, subscribers and authorised users ("Users"), for small-scale personal, non-commercial use provided that all copyright, trade and service marks and other proprietary notices are maintained. By accessing, sharing, receiving or otherwise using the Springer Nature journal content you agree to these terms of use ("Terms"). For these purposes, Springer Nature considers academic use (by researchers and students) to be non-commercial.

These Terms are supplementary and will apply in addition to any applicable website terms and conditions, a relevant site licence or a personal subscription. These Terms will prevail over any conflict or ambiguity with regards to the relevant terms, a site licence or a personal subscription (to the extent of the conflict or ambiguity only). For Creative Commons-licensed articles, the terms of the Creative Commons license used will apply.

We collect and use personal data to provide access to the Springer Nature journal content. We may also use these personal data internally within ResearchGate and Springer Nature and as agreed share it, in an anonymised way, for purposes of tracking, analysis and reporting. We will not otherwise disclose your personal data outside the ResearchGate or the Springer Nature group of companies unless we have your permission as detailed in the Privacy Policy.

While Users may use the Springer Nature journal content for small scale, personal non-commercial use, it is important to note that Users may not:

- 1. use such content for the purpose of providing other users with access on a regular or large scale basis or as a means to circumvent access control:
- 2. use such content where to do so would be considered a criminal or statutory offence in any jurisdiction, or gives rise to civil liability, or is otherwise unlawful;
- 3. falsely or misleadingly imply or suggest endorsement, approval, sponsorship, or association unless explicitly agreed to by Springer Nature in writing:
- 4. use bots or other automated methods to access the content or redirect messages
- 5. override any security feature or exclusionary protocol; or
- 6. share the content in order to create substitute for Springer Nature products or services or a systematic database of Springer Nature journal content.

In line with the restriction against commercial use, Springer Nature does not permit the creation of a product or service that creates revenue, royalties, rent or income from our content or its inclusion as part of a paid for service or for other commercial gain. Springer Nature journal content cannot be used for inter-library loans and librarians may not upload Springer Nature journal content on a large scale into their, or any other, institutional repository.

These terms of use are reviewed regularly and may be amended at any time. Springer Nature is not obligated to publish any information or content on this website and may remove it or features or functionality at our sole discretion, at any time with or without notice. Springer Nature may revoke this licence to you at any time and remove access to any copies of the Springer Nature journal content which have been saved.

To the fullest extent permitted by law, Springer Nature makes no warranties, representations or guarantees to Users, either express or implied with respect to the Springer nature journal content and all parties disclaim and waive any implied warranties or warranties imposed by law, including merchantability or fitness for any particular purpose.

Please note that these rights do not automatically extend to content, data or other material published by Springer Nature that may be licensed from third parties.

If you would like to use or distribute our Springer Nature journal content to a wider audience or on a regular basis or in any other manner not expressly permitted by these Terms, please contact Springer Nature at

onlineservice@springernature.com